Evolution of the infrared properties of the Mount Pinatubo aerosol cloud over Laramie, Wyoming

Steven T. Massie,[1] Terry Deshler,[2] Gary E. Thomas,[3] John L. Mergenthaler,[4] and James M. Russell III[5]

Abstract. Particle size distributions measured from May 1991 to April 1994 over Laramie, Wyoming, are used in Mie calculations to model the wavelength dependence and the time evolution of the extinction, single-scattering albedo, and asymmetry parameters of stratospheric sulfate particles. The calculations cover the time period from 45 days before to 1080 days after the eruption of Mt. Pinatubo. The time evolution of the particle size distribution parameters and the evolution of the infrared extinction are examined concurrently and interrelated in terms of the variables present in the Mie equation for the extinction coefficient. The calculations are validated by comparing the theoretical model values to extinction measurements obtained by the Cryogenic Limb Array Etalon Spectrometer (CLAES), Improved Stratospheric and Mesospheric Sounder (ISAMS), Halogen Occultation Experiment (HALOE), and Stratospheric Aerosol and Gas Experiment (SAGE II) experiments. The Wyoming size distributions are also used to derive simple mathematical expressions from which area and volume densities can be estimated using CLAES extinction measurements.

1. Introduction

The eruption of Mt. Pinatubo in June 1991 produced between 20 and 30 Mt of new stratospheric aerosol [*McCormick and Veiga*, 1992]. The sulfate aerosol cloud had an appreciable impact upon visible and infrared remote sensing instruments by increasing optical depths along limb-viewing and nadir-viewing geometries. The Pinatubo aerosol is being studied due to its impact upon the meridional circulation, the radiation field (e.g., changes in ozone photolysis rates), and the chemistry of the stratosphere (e.g., through heterogeneous chemical reactions upon sulfate aerosol) [*Tie et al.*, 1994; *Hanson et al.*, 1994].

The calculations in this paper complement and expand upon earlier studies of the infrared characteristics of the stratosphere, at times of low (background) aerosol loading and at times after the eruptions of El Chichon (March 28, 1982) [*Thomas et al.*, 1983; *Halperin and Murcray*, 1987; *Pollack et al.*, 1991; *Rusch et al.*, 1994; *Eparvier et al.*, 1994] and Mt. Pinatubo (June 15, 1991) [*Hervig et al.*, 1993; *Lambert et al.*, 1993; *Grainger et al.*, 1993; *Mergenthaler et al.*, 1993; *Massie et al.*, 1994; *Rinsland et al.*, 1994]. The optical and infrared properties of the atmosphere (e.g., the extinction, scattering, absorption, single-scattering albedo, and asymmetry parameters) have been calculated for a range of aerosol amount [*Jursa*, 1985; *d'Almeida et al.*, 1991] and

have been incorporated into computer codes [*Kneizys et al.*, 1988].

It is useful to know how the infrared properties of the sulfate aerosol change as a function of wavelength, altitude, and time. As discussed by *Lacis et al.* [1992], climate forcing by stratospheric aerosols is a function of particle size, and the absorptive properties of the aerosol. As an aid to climate, chemical, and observational studies, particle size distributions, measured at altitudes between 10 and 35 km over Laramie, Wyoming, from May 1991 to April 1994, are used in Mie calculations to model the temporal and wavelength dependence of the aerosol extinction, single-scattering albedo, and asymmetry parameters between 0.36 and 25.0 μm (400 to 27800 cm⁻¹). The time evolution of the particle size distribution parameters for the primary and secondary particle modes, and the evolution of the area and volume densities of the aerosol, are discussed in section 2. The time evolution of the particle size distribution parameters, and the evolution of the infrared extinction, are examined concurrently, and interrelated in terms of the variables present in the Mie equation for the extinction coefficient. The Mie calculations in section 3 are based upon the Wyoming size distributions, and the indices of refraction of H_2SO_4/H_2O liquid droplets. In section 4 the theoretical calculations are validated by comparing them with observations from the Cryogenic Limb Array Etalon Spectrometer (CLAES), Improved Stratospheric and Mesospheric Sounder (ISAMS), and Halogen Occultation Experiment (HALOE) experiments on the Upper Atmosphere Research Satellite (UARS) platform, and with observations by the Stratospheric Aerosol and Gas Experiment (SAGE II) experiment. In section 5 the altitude and temporal dependence of the aerosol extinction at 6.2 μm is discussed. Finally, section 6 presents mathematical expressions from which CLAES aerosol extinction can be used to estimate the area and volume densities of the Mt. Pinatubo aerosol. The expressions are related to those developed and applied by *Grainger et al.* [1995] for application to ISAMS aerosol extinction at 12.1 μm.

---

[1]National Center for Atmospheric Research, Boulder, Colorado.

[2]University of Wyoming, Laramie.

[3]Laboratory for Atmospheric and Space Physics, University of Colorado, Boulder.

[4]Lockheed Martin Palo Alto Research Laboratory, Palo Alto, California

[5]NASA Langley Research Center, Hampton, Viriginia

2. Wyoming Aerosol Size Distributions

Aerosol size distributions, measured over Laramie, Wyoming (41° N, 254° E), are the primary input to the Mie theoretical calculations discussed in section 3. The aerosol measurements were made at altitudes between 10 and 35 km, and cover the period from May 1991 to April 1994. These measurements extend 1 year past the measurement period discussed by *Deshler et al.* [1993]. Observations were made bimonthly from August 1991 to May 1992, and monthly after June 1992. Determination of the size distribution parameters were obtained from the balloon flight data at every 1-km step in altitude. There are a total of 850 size distributions in the Wyoming data set. Since Mt. Pinatubo erupted during June 14-16, 1991, the May and early June 1991 size distribution measurements are for background (low-aerosol loading) conditions. As discussed by *Deshler et al.* [1993], the balloon-borne aerosol instruments measured at each altitude level the total number concentrations of aerosol with radii in the 0.15 to 10 μm range. and the particle size distribution was determined from measurements of the particle concentrations with respect to eight size ranges between 0.15 and 2.0 μm. No particles greater than 1.5 μm were observed.

The particle size distributions for the aerosol are expressed by a sum of lognormal distributions for the primary and secondary size distribution modes. The two modes are expressed in terms of the modal total number density (N_i, particles/cm³), median radius (r_i, μm), and distribution width (σ_i, dimensionless). At each observation altitude, the size distribution (dn/dr, particles cm⁻³ μm⁻¹) is given by the sum of lognormal distributions ($i=1,2$)

$$dn_i/dr = N_i (r s_i (2\pi)^{1/2})^{-1} \exp(-\alpha_i^2/2)$$ (1)

with

$$\alpha_i = \ln (r/r_i)/s_i$$ (2)

$$s_i = \ln (\sigma_i)$$ (3)

$$r = \text{particle radius (μm)}$$ (4)

The particle size distribution specifies the number of particles per cm⁻³ per μm increment of particle radius, at a particle radius of r μm. Integrals of the size distribution over the volumes and areas of the particles yield the expressions

$$A_i = 4 \pi r_i^2 N_i \exp (2 s_i^2)$$ (5)

for the area density (μm² cm⁻³), and

$$V_i = (4/3) \pi r_i^3 N_i \exp (9 s_i^2/2)$$ (6)

for the volume density (μm³ cm⁻³). These volume and area densities are of physical interest, since they are important quantities in calculations of heterogeneous chemistry (i.e., reaction rates which take place upon and inside sulfate aerosol particles).

For each altitude level the values for the size distribution parameters are selected to minimize the difference between the calculated and measured number concentrations for each of the eight size ranges between 0.15 and 2.0 μm. The size distribution parameters yield surface area and mass concentrations which agree with the measurements usually within 10 to 20%, with maximum variations of 30 to 40%.

The calculations in this paper use equations of the form 1-6 to represent the size distributions measured by the Wyoming balloon-borne particle counters. Occasionally, the width of the primary mode made a dominant contribution to the size distribution at for example; 2 μm. (This situation is not desired, since the secondary mode parameters are in agreement with the particle densities for the large particle size ranges). For these cases, an exponential cutoff was used to decrease the primary mode contribution to a value less than that of the secondary mode, at radii typically greater than 0.5 μm. The exponential cutoff produced a smooth particle size distribution, and the distribution had a large particle tail which was determined by the secondary mode parameters. Such adjustments are in effect for the curve labeled "128 days" in Figure 1.

Figure 1 displays the particle size distributions at three representative times for pressures between 40 and 46 hPa (altitudes near 21 km). In Figure 1, the curves labeled -23, 128, and 943 days denote the number of days from the eruption of Mt. Pinatubo and correspond to calendar dates of May 28, 1991, October 21, 1991, and January 10, 1994, respectively. For days 128 and 943, there are noticeable secondary particle modes (near 0.5 and 0.4 μm). It is apparent that there are more smaller particles before the eruption, and there is a significant increase of large particles after the eruption. As discussed by *Deshler et al.* [1993], the secondary modes have integrated number densities roughly equal to the pre-eruption concentration of 0.15-μm particles at altitudes between 15 and 25 km, that is; the secondary modes probably arise from condensation and growth of the sulfuric acid vapor on the larger particles of the background aerosol. In the following paragraphs, the time evolution of the aerosol density, radii, distribution width, area and volume densities, and the infrared extinction, is interpreted in terms of the primary and secondary mode parameters. Changes in both sets of mode parameters increase the magnitude of the aerosol extinction, area and volume densities, following the volcanic eruption. To understand the quantitative origin of these enhancements, it is necessary to examine the changes in the size distribution parameters of both modes.

Particle size distributions
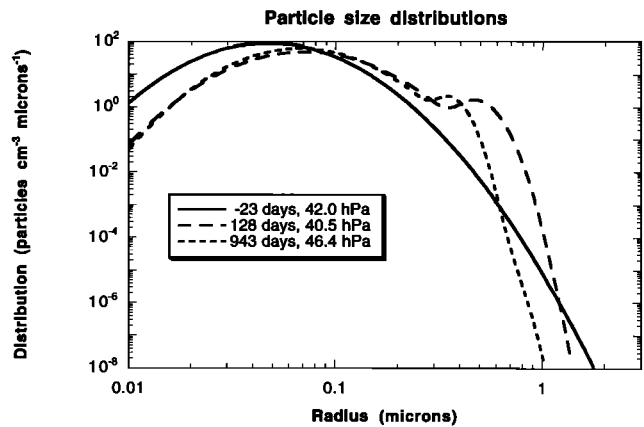
Figure 1. Particle size distributions measured over Laramie, Wyoming, at -23, 128, and 943 days from the Mt. Pinatubo eruption (on May 21, 1991, October 21, 1991, and January 10, 1994) for pressures between 40 and 46 hPa (altitudes near 21 km). Secondary mode maxima are present in the distributions at 128 and 943 days past the Mt. Pinatubo eruption.

Figures 2a - 2c present averages of the size distribution parameters for the 25 - 50 hPa pressure range, as a function of days before and after the Mt. Pinatubo eruption. In Figure 2a, the total and modal particle densities are graphed. Standard

Mode particle density (cm⁻³), 50 - 25 hPa

Mode radii (microns), 50 - 25 hPa

Mode distribution widths, 50 - 25 hPa
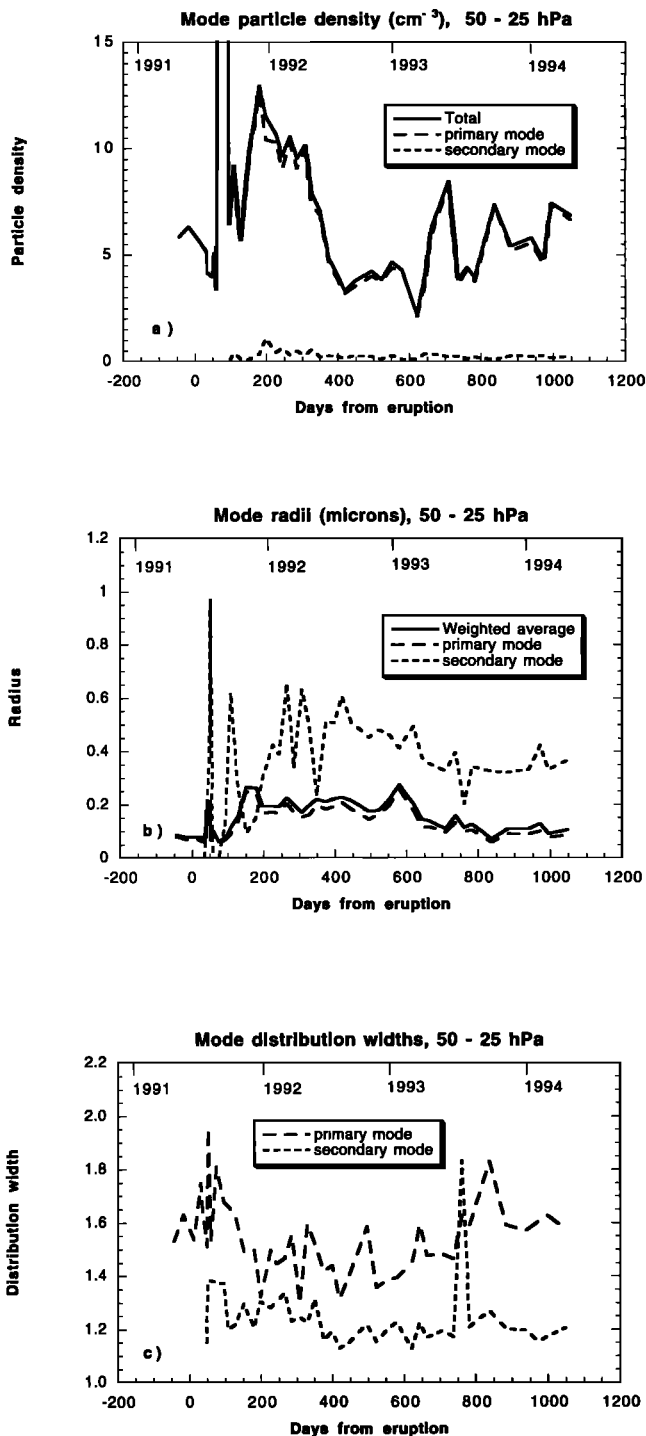
Figure 2. (a) Particle densities (cm⁻³) averaged over the 25 - 50 hPa range for the primary and secondary particle modes. The (off scale) total density on day 75 is 42 cm⁻³. (b) Median radii (μm) for the two distribution modes averaged over the 25 - 50 hPa range. (c) Mode distribution widths (σ's, dimensionless) averaged over the 25 - 50 hPa range for the primary and secondary particle modes. Standard deviations of the averages are represented by solid vertical lines.

deviations of the averages are represented by solid vertical lines. (For other representations of the Wyoming data, see *Deshler et al.* [1993]). It is apparent that most of the particles are contained in the primary mode. Total densities typically range between 5 and 10 cm⁻³. The particles on day 75 (August 29, 1991), whose number densities are off the y axis scale, had an average number density of 42 particles/cm³. Although quite high number densities (> 100 cm⁻³) are seen in thin layers after large volcanic eruptions [*Deshler et al.*, 1992; *Hofmann and Rosen*, 1983], the coagulation lifetime of these particles is quite short (30 - 60 days), and the number densities in Figure 2a are within a factor of 3 of the pre-eruption values.

In Figure 2b the median radii for the two modes of the size distribution are presented. The average radius was obtained by weighting the median radii by the mode number densities. The radii of the secondary mode display more variation than the radii of the primary mode. The primary mode median radii are between 0.1 and 0.2 μm, while the secondary mode median radii are mostly between 0.3 and 0.6 μm.

In Figure 2c the mode distribution widths (σ) are displayed. Note that the natural log of these σ are used in the size distribution expressions (1) - (4). The primary mode has a distribution σ near 1.5, while the secondary mode σ is near 1.2. The widths of the secondary modes (see Figure 1 and Figure 4) therefore are narrower than the widths of the primary modes.

Equations (5) and (6), in conjunction with the size distribution parameters, provide area and volume densities associated with the particle size distributions at each observation altitude. Averages of these area and volume densities, for the 25 to 50 hPa pressure range, are presented in Figures 3a and 3b. Standard deviations of the averages are represented by solid vertical lines. The primary mode contributes the most to the area and volume densities. The decays of the total area and volume densities in Figures 3a and 3b are approximately exponential with time, with e-folding times of approximately 305 days. This timescale is comparable to those of other volcanic eruptions. Lidar studies by *McCormick et al.* [1978] noted an e-folding time of 352 days for the decline of the Volcan de Fuego aerosol, and McCormick and Swissler (section 10.4.1.2 of *WMO*, 1988) found e-folding times between 300 and 330 days from lidar and extinction data in the northern hemisphere following the eruption of El Chichon.

For pressures greater than 50 hPa, there are observations for which the total number densities are much larger than those presented in Figure 2a. For the time period 31 to 95 days after the eruption, the largest total number densities are between 200 and 413 cm⁻³, the surface areas are between 5 and 30 μm² cm⁻³, and the volume densities are between 0.2 and 3 μm³ cm⁻³. For these observations (at altitudes between 15 and 19 km), the primary mode σ vary between 2.0 and 2.5, and the secondary σ vary between 1.1 and 2.1.

3. Mie Calculations

Mie theory was used to model the wavelength dependence of the aerosol extinction, scattering, absorption, single-scattering albedo, and asymmetry parameter for each of the particle size distribution measurements. In the calculations it was assumed that the aerosol particles were composed of H_2SO_4/H_2O in the liquid state. This assumption is

Mode area densities (microns² cm⁻³)
50 - 25 hPa

Mode volume densities (microns³ cm⁻³)
50 - 25 hPa
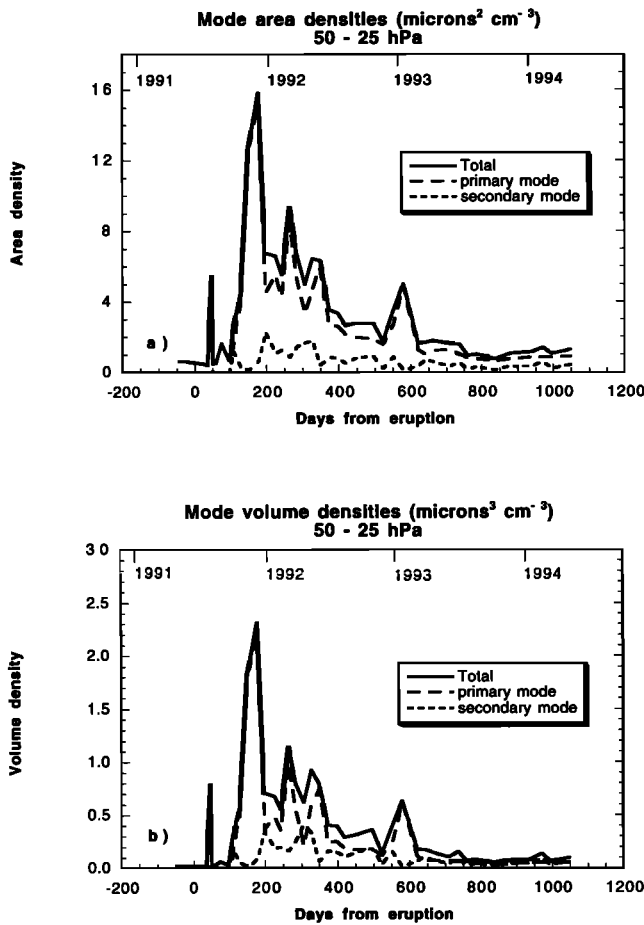
Figure 3. (a) Area densities (μm² cm⁻³) averaged over the 25 - 50 hPa range for the primary and secondary particle modes. (b) Volume densities (μm³ cm⁻³) averaged over the 25 - 50 hPa range for the primary and secondary particle modes. Standard deviations of the averages are represented by solid vertical lines.

appropriate for the range of temperature (206 to 260 K) of the measurements. The composition of H_2SO_4/H_2O is also reasonable since analytical electron microscope analysis of aerosol collected over Laramie, Wyoming, on July 26, July 30, and August 14, 1991, indicates that a large majority (> 99%) of the fine particles in the collected samples were submicrometer aqueous H_2SO_4 droplets [*Sheridan et al.*, 1992].

The calculations do not consider the possibility that the particles have an ash (silicate) component. The samples collected by *Sheridan et al.* [1992] did contain a few particles in the 1 to 10 μm range which were composed of sulfate/crustal material. In a similar study, *Pueschel et al.* [1994] discuss particle size measurements of Mt. Pinatubo aerosol particles for the January to March, 1992 time frame (200 to 290 days after the eruption). Also, 15% of the particle size distributions, observed in March of 1992 at 19 km altitude, and at latitudes between 26° N and 31° N, had a large-particle mode with geometric mean radius near 0.8 μm. X ray energy-dispersive analysis determined an elemental composition of these particles to be mineral ash. The 66% of the particle size distributions observed in January, February, and March 1992 at DC-8 flight altitudes between 10 and 13 km, and latitudes

between 42° N and 87° N, also had a large-particle mode. If the Wyoming measurements missed any large particles, then the theoretical calculation of the extinction coefficient would underestimate the magnitude of the actual extinction.

By Mie theory, the aerosol extinction coefficient b_{ext} (km⁻¹) is given by the expression

$$b_{ext}(\lambda) = 1.0 \times 10^{-3} \int Q_{ext}\ (x,\ m(\lambda))\ \pi\ r^2\ (dn/dr)\ dr \quad (7)$$

where

$$\lambda = \text{wavelength (μm)} \quad (8)$$

$$x = 2\ \pi\ r/\lambda\quad \text{the Mie size parameter} \quad (9)$$

$$m(\lambda) = m_{real} + i\ m_{imag}\quad \text{the complex index of refraction} \quad (10)$$

with real (m_{real}) and imaginary (m_{imag}) indices of refraction, and

$$Q_{ext} = \text{Mie efficiency factor for extinction (dimensionless)}(11)$$

There are similar expressions for the absorption and scattering coefficients, and the coefficients are related by the equations

$$Q_{ext} = Q_{abs} + Q_{sca} \quad (12)$$

and

$$b_{ext} = b_{abs} + b_{sca} \quad (13)$$

Inputs to the calculations are the indices of refraction of the H_2SO_4/H_2O droplets (discussed below), and the particle size distribution (given by (1) - (4)).

An important quantity in radiative transfer calculations is the ratio of b_{sca} and b_{ext}, the single-scattering albedo (ω, dimensionless). Particles with ω equal to unity purely scatter light, while particles with ω equal to zero purely absorb light. Another important quantity, the asymmetry factor, g, is given by the equation

$$g = (1/2) \int_{-1}^{+1} P(\cos\theta)\ \cos\theta\ d\cos\theta \quad (14)$$

The phase function P gives the angular distribution of scattered energy for the aerosol particle, where θ is the angle between the incident beam and the scattered beam [*Liou*, 1980]. For $\theta=0°$ light is scattered in the forward direction, and for $\theta=180°$ light is scattered in the backward direction, so g is positive for a predominance of forward scattering, and g is negative for a predominance of backward scattering. The use of these parameters are discussed thoroughly in the radiative transfer literature [i.e., *Liou*, 1980; *Hansen and Travis*, 1974].

The aerosol extinction coefficient, b_{ext}, is a sensitive function of the particle radius. The integrand of (7) at 1600 cm⁻¹, for the size distribution illustrated in Figure 1 for e.g., 128 days after the Mt. Pinatubo eruption, has a maximum near 0.5 μm, corresponding to the secondary particle mode. Though the particle size distribution of the secondary mode in Figure 1 has a peak value a factor of 100 less than the primary mode peak value, the r^2 and Q_{ext} terms in (7) increase by factors of 39 and 5 as particle radii increase from 0.08 to 0.5 μm. Therefore, the infrared extinction is quite sensitive to the presence of large particles, represented in the size distribution by the particles in the secondary mode. On average, the primary mode contributes 65% to the b_{ext} integral, and the

secondary mode contributes 35% to b_{ext}, for the 50 - 25 hPa pressure range, from 100 to 1000 days past the Pinatubo eruption.

When the integrand of (7) is divided by the particle volume, the ratio is nearly constant for most of the particle range. This allows one to approximate (7) by the expression

$$b_{ext}(\lambda) = C_{ratio} \int (4/3) \pi r^3 \, (dn/dr) \, dr \qquad (15)$$

$$= C_{ratio} V \qquad (16)$$

where

$$C_{ratio} = (\pi r^2 Q_{ext}) / ((4/3) \pi r^3) \qquad (17)$$

and V is the volume density (sum of $V_1 + V_2$ from (6)). Equation (16) is derived and used by Grainger et al. [1995] to relate extinction and volume density for 12.1 μm aerosol extinction observed by the ISAMS experiment on UARS. The reason the volume ratio is nearly constant is that absorption is more important than scattering as the Mie size parameter (x) approaches zero (if the refractive index is complex), since Q_{sca} has an x^4 dependence, and Q_{abs} for small x values (particles in the Rayleigh regime) has the form [van de Hulst, 1957].

$$Q_{abs} = -4 (2\pi r/\lambda) \, Im \, ((m(\lambda)^2 - 1)/(m(\lambda)^2 + 2)) \qquad (18)$$

Thus the $\pi r^2 Q_{abs}$ term has an r^3 dependence. In section 6, we use expressions similar to those of Grainger et al. [1995] to derive relations between extinction and volume density for wavelengths between 5.2 and 12.8 μm for extinction data observed by the CLAES experiment on UARS.

An important input to the theoretical calculations are the indices of refraction of the H_2SO_4/H_2O liquid droplets. The indices of refraction are a function of the H_2SO_4 concentration, which is a function of temperature and the H_2O vapor pressure [Steele and Hamill, 1981; Yue et al, 1986]. For the Wyoming observations, the H_2SO_4 concentration varies between 50 and 88%, with most acidities between 70 and 80%. For sulfate particles in the polar regions, the percent concentration would be in the 40 to 50% range due to the colder temperatures, since the particles take up more H_2O as temperatures decrease.

The H_2SO_4 concentrations are calculated using temperatures and H_2O vapor pressures based upon measurements obtained over Laramie, Wyoming, by the Microwave Limb Sounder (MLS) experiment on the UARS platform. The Steele and Hamill [1981] thermodynamic equilibrium table of temperature, water vapor pressure, and H_2SO_4 concentration is used to calculate the H_2SO_4 concentration. Since the complex indices of refraction are a function of temperature, the temperature dependence of the indices is estimated by application of the Lorentz-Lorenz equation. This correction is modest. Aerosol extinction spectra at 300 and 220 K for 75% H_2SO_4 in the 500 - 2000 cm⁻¹ range differ by roughly 6% (with the 220 K curve being larger in magnitude than the 300 K curve).

The imaginary index becomes very small for wavelengths less than 2.7 μm (wavenumbers greater than 3700 cm⁻¹). At these shorter wavelengths, the particles do not absorb light, and the radiative transfer is that for pure scattering (the single-scattering albedo is unity). For middle infrared instruments, the single-scattering albedo is typically in the range of 1.0 × 10⁻² to 1.0 × 10⁻¹ (discussed below in Figure 8b). Therefore, visible light instruments (e.g., SAGE) observe H_2SO_4

droplets which scatter light, and middle infrared instruments (e.g., the CLAES and ISAMS experiments) observe H_2SO_4 droplets which primarily absorb light.

The present paper relies upon the Palmer and Williams [1975] and Remsberg et al. [1974] indices. Both data sets apply to room temperature conditions. The real indices are in agreement to the 2% level, while the Remsberg imaginary indices are 0 to 60% larger between 747 and 1400 cm⁻¹. Using a particle size distribution at 47.5 hPa, at 128 days past the Mt. Pinatubo eruption, the Remsberg indices yield extinction values approximately 60% larger at 800 cm⁻¹, and nearly the same at wavenumbers greater than 1400 cm⁻¹ (see Figure 4).

In an analysis of Atmospheric Trace Molecule Spectroscopy (ATMOS) transmission spectra, observed on April 1992 at 54° S, Rinsland et al. [1994] compared retrieved sulfate aerosol transmission spectra with theoretical calculations. The theoretical spectrum based upon the Remsberg indices, for wavelengths between 6.25 to 13.3 μm (750-1600 cm⁻¹), gave better agreement with the ATMOS measurements than the spectrum based upon the Palmer and Williams indices, though neither of the theoretical spectra agreed exactly with the ATMOS observations at all wavelengths.

Grainger et al. [1995] comments that modelled radiances, calculated using Wyoming balloon-borne measurements of aerosol distributions, are less than coincident CLAES and ISAMS observed radiances in the 12 μm region. Grainger et al. [1995] used the Remsberg imaginary index at 12 μm in their theoretical calculations, since usage of the Remsberg index reduced the observed discrepancy between modelled and measured values of extinction.

Until the quantitative uncertainties in the indices are resolved, it is useful to be able to convert between theoretical calculations based upon the two sets of laboratory measurements. In Figure 5, the ratios of extinction, scattering, asymmetry factor and single scattering albedo for the two data sets (Remsberg/Palmer and Williams) are displayed. The size distribution used in these calculations is the "128 days" curve of Figure 1. The largest ratios are those for the extinction coefficients, and the smallest ratios are those of the asymmetry factors. For those who wish to use the results derived from
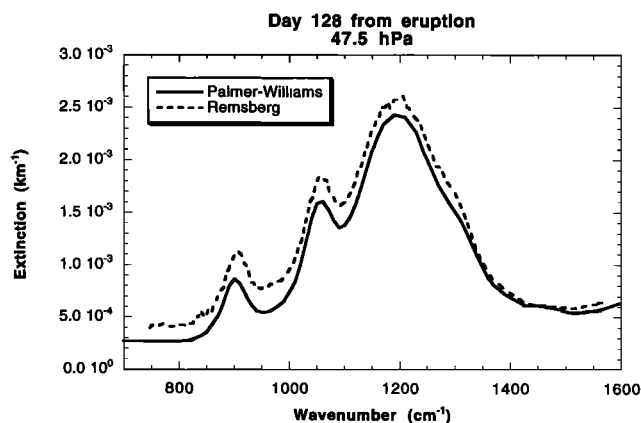
Figure 4. Comparison of sulfate aerosol extinction spectra based upon the Remsberg et al. [1974] and Palmer and Williams [1975] indices of refraction. The size distribution used is the "128 days" curve of Figure 1.
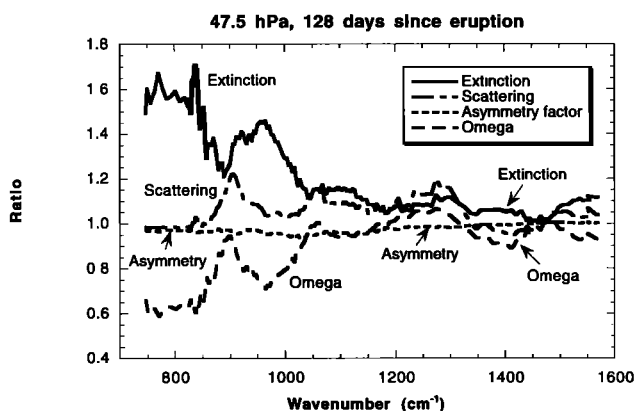
Figure 5. The ratios of extinction, scattering, asymmetry factor, and single scattering albedo for calculations using the Remsberg et al. [1974] and Palmer and Williams [1975] indices between 700 and 1600 cm^{-1} (6.25 - 14.2 μm). The ratios are formed by dividing curves based upon the Remsberg indices by those based upon the Palmer and Williams indices. The size distribution used in the calculation is the "128 days" curve of Figure 1.

calculations based upon the Remsberg indices, the curves in Figure 5 allows one to convert the Palmer and Williams-based values to Remsberg-based values. In section 6, coefficients for the area and volume density expressions are cited for both sets of laboratory data.

Atmospheric extinction curves vary both in magnitude and shape, with the shape of the spectral extinction being a function of the particle radii (via the size distribution) and the H$_2$SO$_4$ content of the droplets (via the temperature, H$_2$O partial pressure, and index of refraction). Figure 6a displays extinction curves for a range of H$_2$SO$_4$ concentrations. The Figure 6a curves were produced by averaging over sets of extinction spectra. The sets at concentrations of 40, 50, 60, 70, and 80% H$_2$SO$_4$ were calculated using an ensemble of size distributions. The ensemble included the Wyoming size distributions measured at all altitudes, at -23, 128, 524, and 943 days from the Mt. Pinatubo eruption.. The value of the aerosol extinction at 1600 cm^{-1} for the 70% H$_2$SO$_4$ case has been used to normalize all of the extinction curves. At 1600 cm^{-1} the imaginary index is fairly constant for the various H$_2$SO$_4$ concentrations, and this is why the curves at 1600 cm^{-1}, in Figure 6a take on similar values. The largest differences in the figure are seen in the peak extinction near 1200 cm^{-1}, and at wavenumbers past 2000 cm^{-1}. Figure 6b and 6c present the single-scattering albedo and asymmetry factors for the curves displayed in Figure 6a. The single-scattering albedos increase in magnitude as wavenumbers increase. There is little sensitivity to the H$_2$SO$_4$ concentration at wavenumbers less than 2000 cm^{-1}. In Figure 6c the asymmetry parameter values increase as wavenumbers increase, and there is little sensitivity to the H$_2$SO$_4$ concentration for the 500 to 3000 cm^{-1} range.
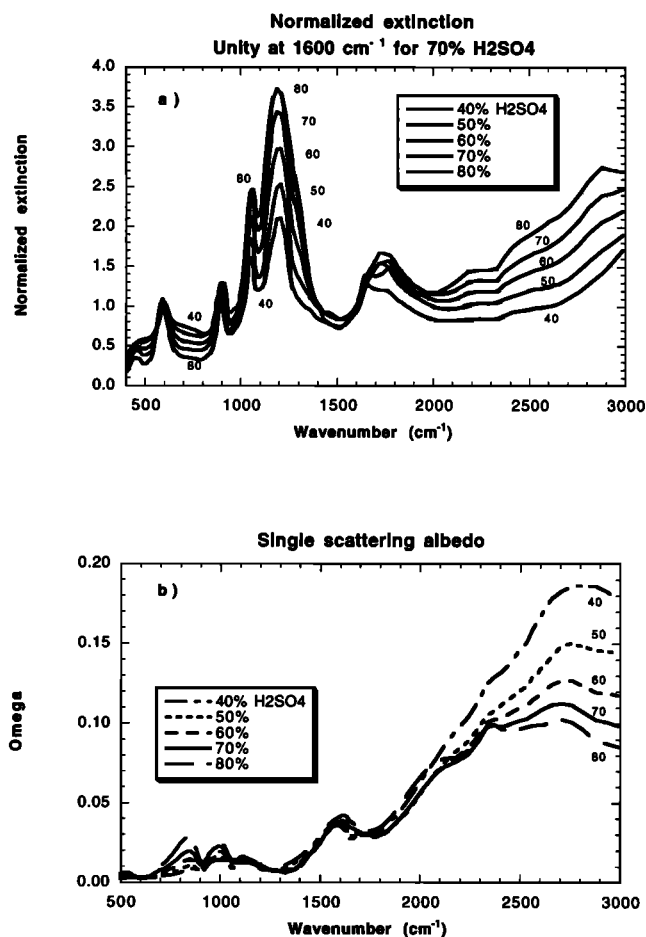
In Figure 6d, the extinction calculations using the Wyoming data for the 100 to 10 hPa range were binned in terms of the weighted distribution average of the particle radius (see Figure 2b), and normalized to unity at 0.525 μm. The figure shows that for the scattering range of wavelengths between 0.525 and 2.7 μm (3700 to 19050 cm^{-1}), the

normalized extinction generally is not a montonic function of the average particle radius. For wavelengths in the absorption range (2.7 - 25 μm), the curves display a weak dependence of normalized extinction versus average particle radius.

The extinction curves in Figure 6a can be used to generate extinction spectra for other times and places. For example, using ISAMS, or CLAES observations at 1605 cm^{-1}, the observed extinction b_{ext} at 1605 cm^{-1} can be used to generate the extinction spectrum $B(v,w)$ throughout the middle infrared by the simple equation

$$B(v,w)=f(v,w) \ (b_{ext}/b_{ref})$$ (19)

where v is wavenumber, w is the H$_2$SO$_4$ concentration (determined by the ambient temperature and H$_2$O vapor pressure), $f(v,w)$ is the curve based upon interpolation of the curves in Figure 6a, and b_{ref} is the value of $f(v,w)$ at 1605 cm^{-1}. This procedure is useful for studies in which estimates of infrared extinction are needed over a range of wavelength.

Figure 6. (a) Theoretical extinction spectra at 40, 50, 60, 70, and 80% H$_2$SO$_4$ based upon calculations using size distributions at all altitudes at -23, 128, 524, and 943 days from the Mt. Pinatubo eruption. All curves have been normalized to the extinction value at 70% H$_2$SO$_4$ at 1600 cm^{-1}. The calculations cover the 400 to 3000 cm^{-1} (3.3 - 25 μm) range. (b) Theoretical single scattering albedos at 40, 50, 60, 70, and 80% H$_2$SO$_4$ based upon calculations using size distributions at all altitudes at -23, 128, 524, and 943 days from the Mt. Pinatubo eruption.

4. Comparison with Observations

The accuracy of (7) and (19) can be checked by comparing CLAES, ISAMS, HALOE, and SAGE extinction, observed over Laramie, Wyoming, with the theoretical extinction model, as a function of time. By comparing the theoretical model to observation for a range of wavelengths from 0.385 to 6.25 μm, the reasonableness and consistency of the wavelength dependence of the theoretical calculations can be assessed. If comparisons at 0.385, 2.45, and 6.25 μm (discussed in the following paragraphs) are satisfactory, then the comparisons give confidence that the theoretical calculations are reasonable.

The Cryogenic Limb Array Etalon Spectrometer (CLAES) experiment on UARS uses tilting Fabry-Perot etalons to observe atmospheric emission between 10 and 60 km altitude [*Roche et al.*, 1993]. CLAES reports measurements of aerosol (and cloud) extinction at 5.27, 6.23, 7.95, 10.83, 11.36, 11.90, 12.65, and 12.82 μm (1897, 1605, 1257, 925, 880, 840, 790, and 780 cm^{-1}, respectively) [*Mergenthaler et al.*, 1993]. The Improved Stratospheric and Mesospheric Sounder (ISAMS) experiment on UARS uses pressure modulated radiometric techniques to observe atmospheric emission [*Taylor et al.*, 1993]. ISAMS measures extinction at 12.1 and 6.3 μm (826 and 1587 cm^{-1}). The Halogen Occultation Experiment (HALOE) on UARS uses radiometer and gas correlation channels to measure gas species mixing ratios and aerosol extinction [*Russell et al.*, 1993]. The HALOE experiment reports aerosol extinction at 2.45, 2.80, 3.40, 3.46, 5.26 μm (4081, 3571, 2941, 2890, and 1901 cm^{-1}). The Stratospheric Aerosol and Gas Experiment (SAGE II) has been measuring aerosol extinction profiles from the Earth Radiation Budget Satellite since October 1984. The SAGE II occultation extinction measurements are made at 1.02, 0.525, 0.453, and 0.385 μm [*Russell and McCormick*, 1989].

Figure 7a compares theoretical extinction at Wyoming at 46 hPa with CLAES (version 7) and ISAMS (version 10) data. The model calculations used the *Palmer and Williams* [1975] indices and have been averaged over the pressure range 41 to 50 hPa. It is apparent that both the CLAES and ISAMS data are in fairly good agreement with the Wyoming data, though the CLAES data is equal to or greater than the theoretical model values. Since UARS was launched 89 days after the eruption of Mt. Pinatubo, the pre-eruption phase of the Wyoming data cannot be compared to the UARS data. The comparison between ISAMS and the Wyoming data is particularly good at 46 hPa.

In the validation study of ISAMS data, *Lambert et al.* [1996] cite systematic and random errors of 10 and 51% at 46hPa. Assuming that the aerosol extinction at a particular location does not vary substantially over an orbital timescale (95 min), comparisons of aerosol extinction profiles, from consecutive UARS orbits, provide a reasonable upper limit to the precision of the extinction retrieval. *Lambert et al.* [1996] calculated precisions at 46 hPa on the order of 30% using this technique. In the validation study of CLAES data, *Massie et al.* [1996] cite precisions (based upon the consecutive orbit technique) between 10 and 25%, instrument biases of 30%, and accuracies between 33 and 43%. As discussed by *Massie et al.* [1995], the archived CLAES extinction data at 1605 cm^{-1} must be corrected for the presence of pressure induced absorption (PIA) due to molecular oxygen. The CLAES data points in Figure 7a reflect this needed adjustment (the PIA
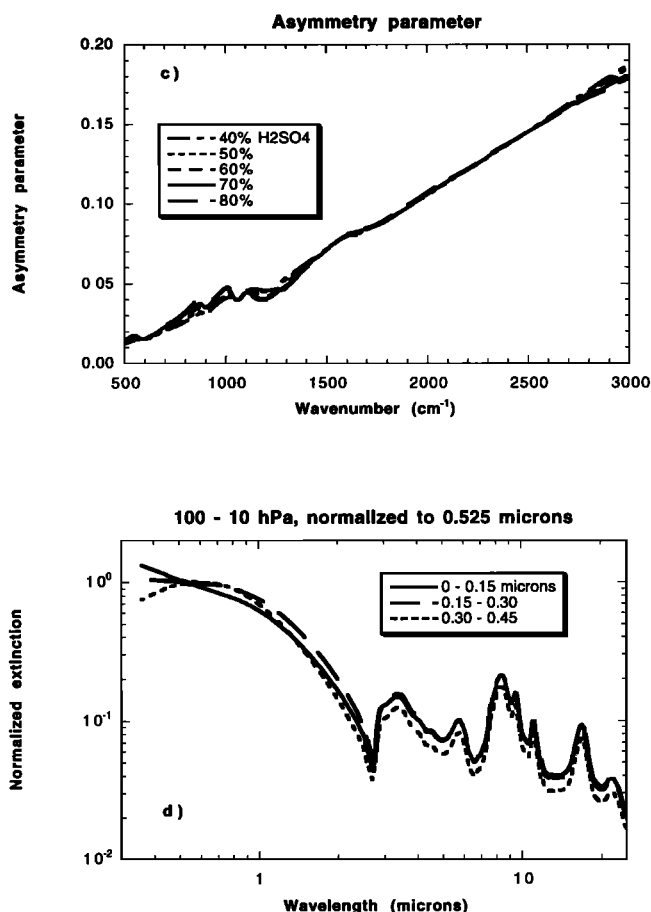

Figure 6. (c) Theoretical asymmetry parameters at 40, 50, 60, 70, and 80% H$_2$SO$_4$ based upon calculations using size distributions at all altitudes at -23, 128, 524, and 943 days from the Mt. Pinatubo eruption. The calculations cover the 400 to 3000 cm^{-1} (3.3 - 25 μm) range. (d) Theoretical extinction curves, binned according to particle radii ranges (μm). All curves have been normalized to unity at 0.525 μm. The curves are based upon averages over the full Wyoming data set for the 100 - 10 hPa range.

contribution was subtracted from the archived data). The ISAMS and CLAES error bars therefore are roughly 50 and 40%, respectively, and are represented in Figure 7a by solid vertical lines. The model values fall within the error bars of the ISAMS and CLAES data presented in Figure 7a.

In Figure 7b HALOE (version 17) data at 4081 cm^{-1} (2.45 μm) is graphed with the theoretical model values. HALOE observations are displayed for the time period 154 to 1302 days after the eruption (December 1991 to January 1995). Agreement between theory and observation is particularly good for times less than 800 days after the eruption. The comparison shows that the HALOE instrument observes over a 3-year time period the factor of 50 decrease in the theoretical aerosol extinction. HALOE error bars are on the order of 20% [*Hervig et al*, 1996].

SAGE 0.385-μm extinction data (archived at the EOS Langley DAC) are compared in Figure 7c to the model calculations. The model values generally track the observations fairly well. These comparisons are in general agreement with SAGE validation papers [*Osborn et al.*, 1989;
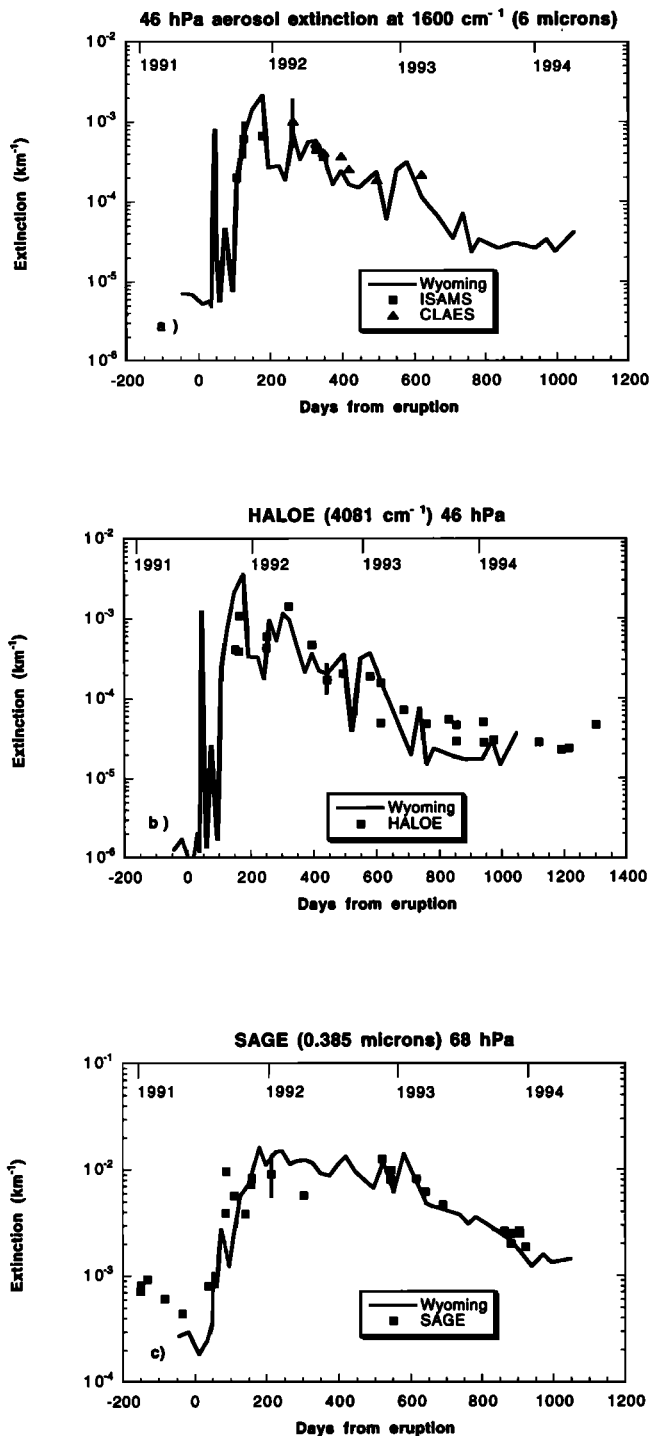
Figure 7. (a) Comparison of theoretical (solid line) and ISAMS and CLAES extinction (km^{-1}) observations over Laramie, Wyoming at 46 hPa, at 1605 cm^{-1} (6.23 μm). The pressure induced absorption due to molecular oxygen has been subtracted from the archived CLAES data. The theoretical curve is based upon particle size measurements in the 41 to 50 hPa range. (b) Comparison of theoretical (solid line) calculations for the 41 - 50 hPa range, and HALOE extinction (km^{-1}) observations over Laramie, Wyoming, at 68 hPa, at 4081 cm^{-1} (2.45 μm). (c) Comparison of theoretical (solid line) calculations in the 63 - 73 hPa range, and SAGE II extinction (km^{-1}) observations over Laramie, Wyoming, at 68 hPa, at 25974 cm^{-1} (0.385 μm).
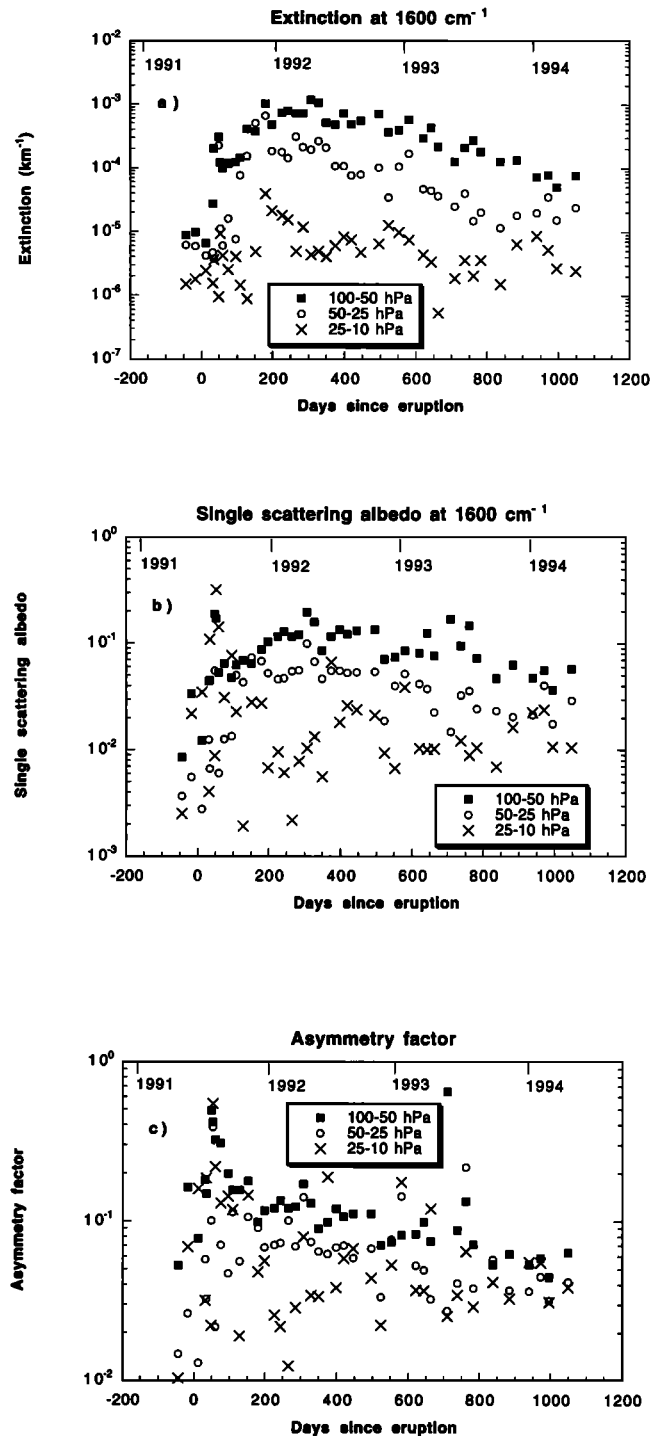
Figure 8. (a) Averages of theoretical extinction (km^{-1}) at 1600 cm^{-1}, as a function of days from the Mt. Pinatubo eruption, for the pressure ranges 25 - 100 hPa, 25 - 50 hPa, and 10 - 25 hPa. (b) Averages of theoretical single scattering albedo (dimensionless) at 1600 cm^{-1}. (c) Averages of theoretical asymmetry factors (dimensionless) at 1600 cm^{-1}.

Oberbeck et al., 1989] which compare the SAGE extinction values to correlative measurements (based upon impactor, dustsonde, lidar, and laser spectrometer probe data).

The comparisons between theory and the SAGE data (near 0.385 μm), the HALOE data (near 2.45 μm), and the ISAMS

Table 1. The Coefficients of Equation (21), for f_{acid}, Based Upon *Palmer and Williams* [1975] Refractive
Indices

Wavenumber, cm^{-1}	Wavelength, μm	Coefficients		
		a	b	c
780	12.82	1.811(0)	2.070(-2)	-8.399(-1)
790	12.66	1.624(0)	3 946(-1)	-1.026(0)
843	11.86	7.425(-1)	1.878(0)	-1.620(0)
880	11.36	-2.022(-1)	3.204(0)	-1.995(0)
925	10.81	6.162(-1)	5.729(-3)	3.696(-1)
1257	7.96	-1.831(-1)	1.310(0)	-1.454(-1)
1605	6.23	5.527(-1)	1.202(0)	-7.675(-1)
1897	5.27	-5.166(-1)	3.132(0)	-1.635(0)

1.811(0) reads 1.811×10^0.

and CLAES data (near 6.25 μm), are consistent in that the error bars of the observations for each of the instruments typically overlap the model values. The comparisons in Figures 7a-7c suggest that extinction spectra, based upon application of (19), will be reasonably accurate.

From Figure 7 the aerosol extinction from the observations and theory yield approximate e-folding times between 200 and 280 days (which is shorter than the e-folding times of 305 days for the area and volume densities discussed in section 2 above). These e-folding times apply to a period of time for which there is an appreciable decrease in the post eruption extinction. The SAGE and HALOE extinction data, at 900 days after the Pinatubo eruption, are within factors of 10 and 30 of the pre-eruption theoretical values, while the pre-eruption theoretical values are factors of 100 and 3000 smaller than the theoretical maxima in Figure 7 at the SAGE and HALOE wavelengths.

5. Altitude-Temporal Characteristics of the Calculations

Altitude-temporal characteristics of the model extinction, single-scattering albedo, and asymmetry parameters, all at 1600 cm^{-1}, are presented in Figures 8a-8c. The extinction data are binned according to three pressure ranges (100-50, 50-25, and 25-10 hPa). For the pressure ranges 100-50 and 50-25 hPa the aerosol extinction rises by a factor of nearly a 100 between the pre and post eruption phases. The 50-25 hPa data falls off with time somewhat faster than the 100-50 hPa data.

For pressures between 25 and 10 hPa there is only a factor of 10 enhancement in the model aerosol extinction between the pre and post eruption phases.

In Figure 8b an increase in the single-scattering albedo, between the pre and post eruption phases, of approximately 15, 20, and 25%, is evident in the 100-50, 50-25, and 25-10 hPa data, respectively. Although there is a lot of scatter in the data at the highest altitudes, the majority of the single-scattering albedos are on the order of 0.1 or less. At 50 days past the eruption, there are observations for which the single-scattering albedos are in the 0.2 to 0.4 range for pressures between 100 and 25 hPa.

In Figure 8c most of the asymmetry factors at 1600 cm^{-1} have values 0.1 or lower. The asymmetry factors for the two highest pressure bins reveal similar decreases with time, while the 25-10 hPa data show a lot of scatter. With values near 0.1 or less, the calculations show that the sulfate aerosol particles have phase functions which scatter light with a slight preference for the forward direction. At 50 days past the Pinatubo eruption, there are observations for which the asymmetry factors are between 0.3 and 0.5.

Examination of graphs similar to Figure 7b (in which the theoretical model values are compared to HALOE data) reveal satisfactory agreement between observation and theory for pressures other than 46 hPa. HALOE 4081 cm^{-1} (2.45 μm) observations at 100 and 68 hPa (not shown), and the 46 hPa observations in Figure 7b, agree well with the theoretical model. At 31 and 21 hPa, the HALOE measurements are somewhat larger than the model. At 21 hPa the HALOE data

Table 2. Coefficients of Equation (23), for r_{log}, Based Upon *Palmer and Williams* [1975] Refractive
Indices

Wavenumber, cm^{-1}	Wavelength, μm	Coefficients		
		d	e	f
780	12.82	-8.991	-1.184(-3)	-1.887(-2)
790	12.66	-8.985	2.733(-3)	-1.844(-2)
843	11.86	-8.790	-1.653(-2)	-2.763(-2)
880	11.36	-8.294	-1.515(-1)	-6 708(-2)
925	10.81	-8.350	-2.094(-1)	-8.517(-2)
1257	7.96	-7.548	-4.855(-1)	-1.557(-1)
1605	6.23	-8.252	-1.692(-1)	-8.838(-2)
1897	5.27	-8.064	-2.342(-1)	-1.103(-1)

-1.184(-3) reads -1.184×10^{-3}.

Table 3. Rms Fits to the Data for the r_e, A, and V Values, Based Upon the Coefficients Presented in Tables 1 and 2

Wavenumber, cm^{-1}	Wavelength, µm	Rms (r_e), %	Rms(A), %	Rms(V), %
780	12.82	20	22	6
790	12.66	20	23	6
843	11.86	20	24	7
880	11.36	20	23	8
925	10.81	20	23	9
1257	7.96	21	22	10
1605	6.23	20	24	11
1897	5.27	20	25	11

These rms values are based upon the exclusion of outliers which are greater than 50, 50, and 100% for the r_e, A, and V fits. Roughly 10% of the 591 input data points for each wavenumber were outliers.

approach an asymptotic value near 6.0×10^{-6} km^{-1}, while the model approaches values between 1 and 4×10^{-6} km^{-1} at times 600 days or more past the Pinatubo eruption. The asymptotic behavior is instrumental in nature, and indicates the lower extinction threshold of the HALOE instrument at 2.45 µm. These comparisons of the HALOE observations with theoretical model values indicate that the theoretical results in Figures 8a-8c are valid, especially for the 100 - 50 and 50 - 25 hPa bins.

6. Volume and Area Densities

Following the work of *Grainger et al.* [1995], mathematical relationships between surface density (A, µm^{-2} cm^{-3}), volume density (V, µm^{-3} cm^{-3}), effective radius (r_e, µm), and extinction (b_{ext}, km^{-1}), can be calculated in a manner which is convenient for applications (via straightforward transformation between aerosol extinction and the desired A, V, r_e values). We use this formalism, with minor changes. Equation (16) is rewritten as

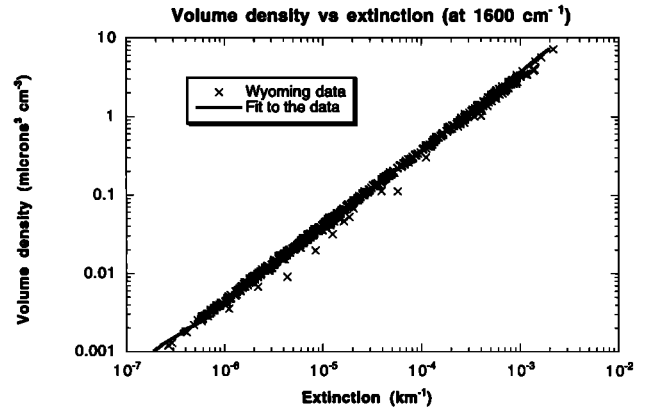$$V = b_{ext} / (f_{acid} \exp(r_{log})) \qquad (20)$$

where

$$f_{acid} = a + b\,H + c\,H^2 \qquad (21)$$

$$H = (H_2SO_4 \text{ concentration}) / 70\% \qquad (22)$$

Volume density vs extinction (at 1600 cm^{-1})

Figure 9. The relationship between theoretical extinction (km^{-1}) at 1600 cm^{-1} (6.25 µm) and the volume density (mm^3 cm^{-3}) for the full Wyoming size distribution data set. The fit to the data set is given by the solid line, and is based upon the coefficients presented in Tables 1 and 2.

$$r_{log} = d + e\,\log_e(r_e) + f\log_e^2(r_e) \qquad (23)$$

with H between 0 and 1.43. The effective radius, r_e, is discussed by *Hansen and Travis* [1974],

$$r_e = 3\ V/A \qquad (24)$$

The area and volume densities are related by

$$A = \alpha V^\beta \qquad (25)$$

where $\alpha = 8.752$ and $\beta = 0.78$. The α and β coefficients were calculated by *Grainger et al.* [1995] by a least squares fit to values of A and V, based upon the ensemble of Wyoming size distributions. Distributions were excluded from the fitting proceedure by *Grainger et al.* [1995] if they did not adequately fit the original measurements. Roughly 10% of the Wyoming data were excluded from the fitting proceedure.

Coefficients a-f for (21) and (23) were calculated at the wavenumbers at which the CLAES experiment reports aerosol extinction, using the full Wyoming ensemble. The coefficients are reported in Tables 1 and 2. To solve for r_e, A, V, (24), (20), and (25) are iterated until convergence, as discussed by *Grainger et al.* [1995], starting with an initial guess for r_e. Table 3 reports the rms percent differences between the original values of r_e, A, V and the calculated values. The

Table 4. Coefficients of Equation (21), for f_{acid}, Based Upon *Remsberg* [1974] Refractive Indices

Wavenumber, cm^{-1}	Wavelength, µm	Coefficients		
		a	b	c
780	12.82	1.843(0)	-2.677(-2)	-8.240(-1)
790	12.66	1.654(0)	3.507(-1)	-1.012(0)
843	11.86	7.776(-1)	1.832(0)	-1.609(0)
880	11.36	-1.832(-1)	3.183(0)	-1.992(0)
925	10.81	6.110(-1)	3.795(-2)	3.425(-1)
1257	7.96	-1.824(-1)	1.303(0)	-1.391(-1)
1605	6.23	5.528(-1)	1.202(0)	-7.676(-1)
1897	5.27	-5.170(-1)	3.133(0)	-1.635(0)

1.843(0) reads 1.843×10^0.

Table 5. Coefficients of Equation (23), for $r_{\log}$, Based Upon *Remsberg* [1974] Refractive Indices

Wavenumber, cm^{-1}	Wavelength, μm	Coefficients		
		d	e	f
780	12.82	-8.619	-8 559(-2)	-4.173(-2)
790	12.66	-8.630	-7.874(-2)	-4.028(-2)
843	11.86	-8.419	-1.054(-1)	-5.123(-2)
880	11.36	-8.121	-1.924(-1)	-7.785(-2)
925	10.81	-8.103	-2.759(-1)	-1.030(-1)
1257	7.96	-7.492	-5.023(-1)	-1.600(-1)
1605	6.23	-8.255	-1.697(-1)	-8.798(-2)
1897	5.27	-8.065	-2.340(-1)	-1.101(-1)

-8.559(-2) reads -8.559×10^{-2}

equations yield rms differences on the order of 25, 10, and 20%. These values refer to rms averages which excluded outliers (i.e., size distributions for which the differences between the original and calculated values were greater than 50, 100, and 100% for r_e, A, and V). Approximately 10% of the Wyoming data were outliers. Figure 9 displays the fit to the volume densities for the full Wyoming ensemble at 1600 cm^{-1}.

The coefficients in Tables 1-2 are calculated using the *Palmer and Williams* [1975] indices. As discussed in section 3, several correlative studies favor the *Remsberg et al.* [1974] indices. Tables 4 and 5 therefore present coefficients based upon the Remsberg indices. Table 6 presents rms percent differences between the iterated values of A, V, and r_e and the original values.

The rms values in Table 6 assume errorless extinction measurements. As discussed, and illustrated in Figures 5 of *Massie et al.* [1996], comparisons of CLAES extinction data with theoretical extinction, calculated using the Wyoming size distribution data, show that the CLAES extinctions are larger than theoretical values, especially at 21 and 31 hPa. Comparisons of CLAES and SAGE extinction data (scaled by the theoretical ratios of extinction at the SAGE and CLAES wavelengths), show similar results (see Figure 7 of *Massie et al.* [1996]). Table 7 presents scaling factors for the CLAES extinction data which rectifies these differences. When these factors are used to multiply CLAES version 7 extinction data, and the coefficients presented in Tables 4 and 5 are used to

Table 6. Rms Fits to the Data for the r_e, A, and V Values, Based Upon the Coefficients Presented in Tables 4 and 5

Wavenumber, cm^{-1}	Wavelength, μm	Rms (r_e), %	Rms(A), %	Rms(V), %
780	12.82	20	23	7
790	12.66	20	23	7
843	11.86	20	23	8
880	11.36	20	23	9
925	10.81	20	23	9
1257	7.96	21	22	10
1605	6.23	20	24	11
1897	5.27	20	25	11

These rms values are based upon the exclusion of outliers which are greater than 50, 50, and 100% for the r_e, A, and V fits. Roughly 10% of the 591 input data points for each wavenumber were outliers.

obtain retrieved CLAES area and volume densities, the average percent differences between the retrieved and the Wyoming volume densities are close to zero, and the rms differences are on the order of 35% for pressures between 100 and 21 hPa. For the area densities, the average and rms differences between the retrieved and Wyoming values are on the order of 16 and 35%. The wavelength dependence of the scaling factors in Table 7 is given by the wavelength dependence of the reciprocals of the ratios presented in Figures 5 and 7 of *Massie et al.* [1996]. Note that the scaling factors deviate substantially from unity.

It is of interest that (25) fits the size distribution data fairly well, considering that six size distribution parameters are required to specify the full distribution. The reason that (25) does this is evident by manipulating (5) and (6). Equations (5) and (6) yield, after some rearrangement, an expression of the form given by (25), where β is two thirds, and α is given by

$$\alpha = (4\pi/(4/3 \pi)^{2/3}) N^{1/3} \exp(2s^2)/((\exp(9s^2/2))^{2/3}) \quad (26)$$

where s is the natural log of σ. The reason that β is equal to two thirds follows from the simple geometrical relationship between the area and volume of a sphere (which is near 0.78, as calculated from the least squares fit of A and V). It is not suprising that the least squares value of β differs from two thirds, since (25) attempts to represent a size distribution that has two modes. Equation (26) shows that α is not a constant, but is dependent upon the values of N and σ. From Figures 2a and 2c, typical values of N and σ are 7 and 1.5 for the primary mode, and 0.2 and 1.2 for the secondary mode. Insertion of these values into (26) yields an (summed) α of 9.88, which is within 15% of the least squares fit value of 8.75.

The calculations in the previous paragraph tell us that application of (25) is limited to a range of N and σ which are similar to those inherent in the Wyoming size distribution ensemble. The equations for r_e, A, and V, however, are likley to be valid at locations away from Laramie, Wyoming. *Grainger et al.* [1995] compared retrieved ISAMS 12.1 μm aerosol surface area altitude profiles to a profile measured near the equator by a UV differential absorption lidar, and obtained good agreement between the two sets of measurements.

7. Conclusions and Applications of the Data

The work above discusses calculations which examine the time evolution of the infrared properties of the Mt. Pinatubo

Table 7. Extinction Scaling Factors

Wavenumber cm^{-1}	Wavelength, μm	Pressure, hPa				
		100	68	46	31	21
780	12.82	0.56	0.78	0.92	0.34	0.12
790	12.66	0.42	0.63	0.69	0.24	0.09
843	11.86	0.68	1.03	1.37	0.42	0.31
880	11.36	0.88	1.50	2.05	1.02	0.46
925	10.81	1.04	1.78	2.15	0.78	0.35
1257	7.96	0.88	0.89	1.27	0.60	0.36
1605	6.23	0.49	0.57	0.77	0.37	0.21

aerosol cloud for a range of wavelength (0.385 to 12 μm) and pressure (from 100 to 10 hPa). The evolution of the particle size distribution parameters and the evolution of the infrared properties are examined concurrently. It is demonstrated that the particle size distribution parameters for the primary and secondary particle modes change after the eruption of Mt. Pinatubo, and that the infrared properties reflect these changes. The primary reason that the extinction is enhanced in the infrared (by a factor of 100 from pre-eruption values) is that the r^2 and Q_{ext} values, which are dependent upon the Mie size parameter $x=2\pi r/\lambda$ in the theoretical expression for the extinction coefficient (b_{ext}), increase substantially after the Pinatubo eruption. Even though the total number densities (e.g., for the 50-25 hPa range, see Figure 2a) do not change substantially after the eruption, the median radii increase (see Figure 2b) for both particle modes, and the r^2 and Q_{ext} values for the secondary mode increase substantially. At times of 300 to 1000 days after the eruption, the mode radii slowly decrease in magnitude, and the extinction values also decrease.

In addition to the particle size distributions, an important input to the Mie calculations are the indices of refraction for H_2SO_4/H_2O liquid droplets. The imaginary indices are uncertain (by up to 60%) at wavenumbers shorter than 1200 cm^{-1} (wavelengths longer than 8.3 μm), based upon comparisons of the imaginary indices of *Palmer and Williams* [1975] and *Remsberg et al.* [1974]. Figure 5 therefore displays curves by which one can convert extinction spectra from those based upon the Palmer and Willams indices to those based upon the Remsberg indices.

Figures 6a-6d can be used to estimate the extinction, single-scattering albedo, and asymmetry parameters over a range of infrared wavelengths. The curves appear to be quite reasonable, since they compare favorably to satellite observations which span the 0.385 to 6.25 μm wavelength range (see Figures 7a-7c). The graphical results presented in Figures 6a-6d are available in electronic form upon request.

The coefficients presented in Tables 1 and 2 (for the Palmer and Williams indices), and Tables 3 and 4 (for the Remsberg indices) can be used in conjunction with CLAES aerosol extinction data to estimate the volume and area densities of the sulfate aerosol. The volume and area densities, obtained by iterating (24), (20), and (25), have rms accuracies of roughly 10 and 25%, respectively, based upon errorless extinction data and laboratory indices. Since (20)-(25) are approximate, it will be useful to apply more refined techniques, such as those of *Rodgers* [1990], to retrieve the area and volume densities.

References

d'Almeida, G. A., P. Koepke, and E. P. Shettle, *Atmospheric Aerosols, Global Climatology and Radiative Characteristics*, A. Deepak, Hampton, Va., 1991.

Deshler, T., D. J. Hofmann, B. J. Johnson, and W. B. Rozier, Ballonborne measurements of the Pinatubo aerosol size distribution and volatility at Laramie, Wyoming, during the summer of 1991, *Geophys. Res. Lett.*, *19*, 199-202, 1992.

Deshler, T., B. J. Johnson, and W. R. Rozier, Balloonborne measurements of Pinatubo aerosol during 1991 and 1992 at 41° N: Vertical profiles, size distributions, and volatility, *Geophys. Res. Lett.*, *20*, 1435-1438, 1993.

Eparvier, F. G., D. W. Rusch, R. T. Clancy, and G. E. Thomas, Solar Mesosphere Explorer satellite measurements of El Chichon stratospheric aerosols, 2, Aerosol mass and size parameters, *J. Geophys. Res.*, *99*, 20,533-20,544, 1994.

Grainger, R. G., A. Lambert, F. W. Taylor, J. J. Remedios, C. D. Rodgers, M. Corney, and B. J. Kerridge, Infrared absorption of volcanic stratospheric aerosols observed by ISAMS, *Geophys. Res. Lett.*, *20*, 1283-1286, 1993.

Grainger, R. G., A. Lambert, C. D. Rodgers, F. W. Taylor, and T. Deshler, Stratospheric aerosol effective radius, surface area, and volume estimated from infrared measurements, *J. Geophys. Res.*, *100*, 16,507-16,518, 1995.

Halperin, B., and D. G. Murcray, Effect of volcanic aerosols on stratospheric radiance at wavelengths between 8 and 13 μm, *Appl. Opt.*, *26*, 2222, 1987.

Hansen, J. E., and L. D. Travis, Light scattering in planetary atmospheres, *Space. Sci. Rev.*, *16*, 527-610, 1974.

Hanson, D. R., A. R. Ravishankara, and S. Solomon, Heterogeneous reactions in sulfuric acid aerosols: A frame work for model calculations, *J. Geophys. Res.*, *99*, 3615-3629, 1994.

Hervig, M. E., J. M. Russell III, L. L. Gordley, J. H. Park, and S. R. Drayson, Observations of aerosol by the HALOE experiment onboard UARS: A preliminary validation, *Geophys. Res. Lett.*, *20*, 1291-1294, 1993.

Hervig, M. E., J. M. Russell III, L. Gordley, J. H. Park, S. Roland Drayson, and T. Deshler, Validation of aerosol measurements from the Halogen Occultation Experiment, *J. Geophys. Res.*, *101*, 10,267-10,275, 1996.

Hofmann, D. J., and J. M. Rosen, Stratospheric sulfuric acid fraction and mass estimate for the 1982 volcanic eruption of El Chichon, *Geophys. Res. Lett.*, *10*, 313-316, 1983.

Jursa, A. S., (ed) Optical and Infrared Properties of the Atmosphere, in *Handbook of Geophysics and the Environment*, chapter 18, Air Force Geophys. Lab., Hanscom AFB, Hanscom, Mass., 1985.

Kneizys, F. X., E. P. Shettle, L. W. Abreu, J. H. Chetwynd, G. P. Anderson, W. O. Gallery, J. E. A. Selby, and S. A. Clough, Users guide to LOWTRAN 7, *Rep. AFGL-TR-88-0177*, Air Force Geophys. Lab., Hanscom AFB, Hanscom, Mass., 1988.

Lacis, A., J. Hansen, and M. Sato, Climate forcing by stratospheric aerosols, *Geophy. Res. Lett.*, *19*, 1607-1610, 1992.

Lambert. A., R. G. Grainger, J. J. Remedios, W. J. Reburn, C. D. Rodgers, F. W. Taylor, J. L. Mergenthaler, J. B. Kumer, S. T. Massie, and T. Deshler, Validation of aerosol measurements by the Improved Stratospheric and Mesospheric Sounder, *J. Geophys. Res.*, *101*, 981 - 9830,1996.

Lambert, A., R. G. Grainger, J. J. Remedios, C. D. Rodgers, M. Corney, and F. W. Taylor, Measurements of the evolution of the Mt. Pinatubo aerosol cloud by ISAMS, *Geophys. Res. Lett.*, *20*, 1287-1290, 1993.

Liou, K-N, An introduction to atmospheric radiation, Academic, San Diego, Calif., 1980.

Massie, S. T. , P. L. Bailey, J. C. Gille, E. C. Lee, J. L. Mergenthaler, A. E. Roche, J. B. Kumer, E. F. Fishbein, J. W. Waters, and W. A. Lahoz, Spectral signatures of Polar Stratospheric Clouds and sulfate aerosol, *J. Atmos. Sci.*, *51*, 3027-3044, 1994.

Massie, S. T., et al., Validation studies using multi-wavelength CLAES observations of stratospheric aerosol, *J. Geophys. Res.*, *101*, 9757-9773,1996.

McCormick, M. P., T. J. Swissler, W. P. Chu, and W. H. Fuller, Post-volcanic stratospheric aerosol decay as measured by lidar, *J. Atmos. Sci.*, *35*, 1296-1303, 1978.

McCormick, M. P., and R. E. Veiga, SAGE II measurements of early Pinatubo aerosols, *Geophys. Res. Lett.*, *19*, 155-158, 1992.

Mergenthaler, J. L., J. B. Kumer, and A. E. Roche, CLAES south-looking aerosol observations for 1992, *Geophys. Res. Lett.*, *20*, 1295-1298, 1993.

Oberbeck, V. R., J. M. Livingston, P. B. Russell, R. F. Pueschel, J. M. Rosen, M. T. Osborn, M. A. Kritz, K. G. Snetsinger, and G. V. Ferry, SAGE II aerosol validation: Selected altitude measurements, including particle micromeasurements, *J. Geophys. Res.*, *94*, 8367-8380, 1989.

Osborn, M. T., J. M. Rosen, M. P. McCormick, P. Wang, J. M. Livingston, and T. J. Swissler, SAGE II aerosol correlative observations: Profile measurements, *J. Geophys. Res.*, *94*, 8353-8366, 1989.

Palmer, K. F., and D. Williams, Optical constants of sulfuric acid; application to the clouds of Venus?, *Appl. Opt.*, *14*, 208-219, 1975.

Pollack, J. B., F. C. Witteborn, K. O'Brien, and B. Flynn, A determination of the infrared optical depth of the El Chichon volcanic cloud, *J. Geophys. Res.*, *96*, 3115, 1991.

Pueschel, R. F., P. B. Russell, D. A. Allen, G. V. Ferry, and K. G. Snetsinger, Physical and optical properties of the Pinatubo volcanic aerosol: Aircraft observations with impactors and a Sun-tracking photometer, *J. Geophys. Res.*, *99*, 12,915-12,922, 1994.

Remsberg, E. E., D. Lavery, and B. Crawford, Optical constants for sulfuric and nitric acids, *J. Chem. Engin. Data*, *19*, 263-265, 1974.

Rinsland, C. P., G. K. Yue, M. R. Gunson, R. Zander, and M. C. Abrams, Mid-infrared extinction by sulfate aerosols from the Mt. Pinatubo eruption, *J. Quant. Spectrosc. Radiat. Transfer*, *52*, 241-252, 1994.

Roche, A. E., J. B. Kumer, J. L. Mergenthaler, G. A. Ely, W. G. Uplinger, J. F. Potter, T. C. James, and L. W. Sterritt, The cryogenic limb array etalon spectrometer (CLAES) on UARS: Experiment description and performance, *J. Geophys. Res.*, *98*, 10,763-10,775, 1993.

Rodgers, C. D., Characterization and error analysis of profiles retrieved from remote sensing measurements, *J. Geophys. Res.*, *95*, 5587-5595, 1990.

Rusch, D. W., R. T. Clancy, F. G. Eparvier, and G. E. Thomas, Solar Mesosphere explorer satellite measurements of El Chichon stratospheric aerosols, 1, Cloud morphology, *J. Geophys. Res.*, *99*, 20,525-20,532, 1994.

Russell, J. M., III, L. L. Gordley, J. H. Park, S. R. Drayson, W. D. Hesketh, R. J. Cicerone, A. F. Tuck, J. E. Freferick, J. E. Harries, and P. J. Crutzen, The halogen occultation experiment, *J. Geophys. Res.*, *98*, 10,777-10,797, 1993.

Russell, P. B., and M. P. McCormick, SAGE II aerosol data validation and initial data use: An introduction and overview, *J. Geophys. Res.*, *94*, 8335-8338, 1989.

Sheridan, P. J., R. C. Schnell, D. J. Hofmann, and T. Deshler, Electron microscope studies of Mt. Pinatubo aerosol layers over Laramie, Wyoming during summer 1991, *Geophy. Res. Lett.*, *19*, 203-206, 1992.

Steele, H. M., and P. Hamill, Effects of temperature and humidity on the growth and optical properties of sulfuric acid-water droplets in the stratosphere, *J. Aerosol. Sci.*, *12*, 517-528, 1981.

Taylor, F. W., et al., Remote sensing of atmospheric structure and composition by pressure modulator radiometry from space: The ISAMS experiment on UARS, *J. Geophys. Res.*, *98*, 10,799-10,814, 1993.

Thomas, G. E., B. M. Jakosky, R. A. West, and R. W. Saunders, Satellite limb-scanning thermal infrared observations of the El Chichon stratospheric aerosol: First results, *Geophys. Res. Lett.*, *10*, 997-1000, 1983.

Tie, X., G. P. Brasseur, B. Briegleb, and C. Granier, Two-dimensional simulation of Pinatubo aerosol and its effect on stratospheric ozone, *J. Geophys. Res.*, *99*, 20,545-20,562, 1994.

World Meteorological Organization, *Report of the International Ozone Trends Panel, 1988*, NASA, Washington, D.C., 1988.

Yue, G. K., M. P. McCormick, and W. P. Chu, Retrieval of composition and size distribution of stratospheric aerosols with the Sage II satellite experiment, *J. Atmos. Ocean. Technol.*, *3*, 371-380, 1986

T. Deshler, University of Wyoming, Laramie, WY (e mail: deshler @grizzly.uwyo.edu)

S. T. Massie, National Center for Atmospheric Research, Boulder, CO (e mail: massie@ncar.ucar.edu)

J. L. Mergenthaler, Lockheed Martin Palo Alto Research Laboratory, Palo Alto, CA,

J. M. Russell III, NASA Langley Research Center, Hampton, VA

G. E. Thomas, Laboratory for Atmospheric and Space Physics, University of Colorado, Boulder, CO (e mail: thomas @alcor.colorado.edu)